1 **Technical note: Efficient imaging of hydrological units below lakes and fjords with a floating, transient**
2 **electromagnetic system (FloaTEM)**

4 Pradip Kumar Maurya[1], Frederik Ersted Christensen[1], M. Andy Kass[1], Jesper B. Pedersen[1], Rasmus R. Frederiksen[1],
5 Nikolaj Foged[1], Anders Vest Christiansen[1], and Esben Auken[1,2]

6 [1]Department of Geoscience, HydroGeophysics Group Aarhus University, C.F. Møllers Alle, 4, Aarhus C, Denmark

7 [2]The Geological Survey of Denmark and Greenland (GEUS) Oester Voldgade 10 1350 Copenhagen K Denmark, formerly at 1.

8 Corresponds to: pradip.maurya@geo.au.dk

9 **Abstract**

10 ~~Imagining~~Imaging geological layers beneath lakes, rivers, and shallow seawater provides detailed information critical for
11 hydrological modelling, geologic studies, contaminant mapping, and more. However, significant engineering and
12 interpretation challenges have limited the applications, preventing widespread adoption in aquatic environments. We have
13 developed a towed transient electromagnetic (tTEM) system to a new, easily configurable floating, transient
14 electromagnetic instrument (FloaTEM) capable of imaging the subsurface beneath both fresh and saltwater water bodies.
15 Based on the terrestrial tTEM instrument, the FloaTEM system utilizes a similar philosophy of a lightweight towed
16 transmitter with a trailing, offset receiver, pulled by a small boat. The FloaTEM system is tailored to the specific fresh or
17 saltwater application as necessary, allowing investigations down to 100 m in freshwater environments, and up to 20 m on
18 saline waters. Through synthetic analysis we show how the depth of investigation of the FloaTEM system greatly depends
19 on the resistivity and thickness of the water column. The system has been successfully deployed in Denmark for a variety
20 of hydrologic investigations, improving the ability to understand and model processes beneath water bodies. We present
21 two freshwater applications and a saltwater application. Imaging results reveal significant heterogeneities in the sediment
22 types below the freshwater lakes. The saline water example demonstrates that the system is capable to identify and
23 distinguish clay and sand layers below the saline water column.

24 **1. Introduction**

25 Understanding interactions between surface water and groundwater is necessary for effective management of water
26 resources as they are both part of an interconnected hydrologic system (Sophocleous, 2002; Winter et al., 1998; Harvey
27 and Gooseff, 2015). This requires knowledge of hydrogeological settings below the water column of lakes, streams, and
28 other water bodies, in addition to properties underlying adjacent onshore areas. Non-invasive geophysical methods
29 provide spatial information on these subsurface properties and processes across many environments; over the last few
30 decades the methods have played a vital role in near-surface investigations (Barker, 1980; Hatch et al., 2010a; Day-Lewis
31 et al., 2006). However, deployment of surface-based geophysical investigations (as opposed to airborne systems) on
32 water bodies has historically been difficult (Sheets and Dumouchelle, 2009; Briggs et al., 2019; Parsekian et al., 2015);
33 while not insurmountable, this has limited the application range to some degree.

34 Electrical and electromagnetic methods (EM) are the two most-extensively used geophysical exploration and
35 characterization techniques for hydrologic applications (Binley and Kemna, 2005; Danielsen et al., 2003; Christiansen et

36 al., 2006; Auken et al., 2003; Minsley et al., 2021; Siemon et al., 2009). While classically used on land, several studies
37 have shown that these methods can also be used on lakes, streams, or rivers. Among the electrical methods, electrical
38 resistivity tomography (ERT) has been a common and robust technique, with applications to aquatic environments
39 including mapping the distribution of clay sediments, mapping freshwater saturation in saltwater bay sediments (Manheim
40 et al., 2004), and estimating sediment thicknesses and locating faults (Kwon et al., 2005). These studies deployed
41 relatively long floating cable layouts, or streamers, of approximately 100 meters, towed by a boat for collecting continuous
42 resistivity data. Longer cable layouts, giving deeper information, limit the operational efficiency significantly. This
43 implies that these instruments inherently have a limited depth of investigation (DOI).

44 Applications of transient electromagnetic (TEM) and frequency domain EM tools are reported in previous studies, e.g.,
45 discharge of groundwater to lakes and brines (Ong et al., 2010; Briggs et al., 2019), and extraction of lithium from large
46 scale natural brine systems (Munk et al., 2016). Airborne techniques have proved capable of mapping beneath lakes,
47 rivers and near-shore seas (Fitterman and Deszcz-Pan, 1998; Dickey, 2018; Rey et al., 2019), but are costly and provide
48 lower vertical and lateral resolution than their ground-based counterparts (Hatch et al., 2010b).

49 There has been a growing interest in the development of a towed, waterborne EM system, as such an instrument provides
50 continuous information with high lateral resolution. Mollidor et al. (2013) have shown an application of a commercial
51 in-loop transient EM (TEM) system on a volcanic lake to map sediment thickness. Since the system had a large transmitter
52 loop (18x18 m^2), they encountered non 1D-effects requiring 3D modelling for proper interpretation. Hatch et al. (2010b)
53 presented results from a waterborne survey where they used a floating setup of a commercial TEM system, used over a
54 40 km section of the Murray River (Australia) to monitor the influx of saline water. Micallef et al. (2020) and Gustafson
55 et al. (2019) used control source electromagnetic systems for hydrogeologic applications in shallow sea water. These
56 studies and systems, while effective, have limitations preventing their widespread use in waterborne applications,
57 specifically in terms of limited DOI and horizontal resolution. An ideal system would be compact and lightweight, have
58 a small footprint, and provide sufficient transmitter power to investigate the hydrogeological properties beneath the water
59 column.

60 Recent advancements in electronics of EM instrumentation led Auken et al. (2018) to develop a ground-based towed
61 transient electromagnetic system (tTEM) for efficient and high resolution 3D mapping of the subsurface (Maurya et al.,
62 2020). The tTEM system provides the necessary framework for creating a floating, towed EM system. The tTEM-system
63 is relatively compact, with the entire system extending no more than 16 m behind the towing vehicle and a maximum
64 width of 4 m. It has high lateral resolution, down to 10 m x 10 m. The tTEM also has a relative high transmitter moment
65 for such a compact system, providing depths of investigation in ground-based surveys down to 100m. The waterborne
66 version of the tTEM system is referred to as FloaTEM (see Fig.1)– and a recent application of the FloaTEM system has
67 been presented by Lane et al. (2020) where they successfully used the ground configuration of the system on rivers and
68 estuaries in the United States to characterize the underlying hydrological system. In their study the system was used as it
69 was designed for ground-based applications (Auken et al., 2018) without any modifications to actual geometry and
70 measurementsmeasurement protocols. In this paper, we present a greatly improved and a flexible version of the FloaTEM
71 system to investigate subsurface properties beneath both fresh and saline water columns. We highlight the design aspects
72 of the system and discuss capabilities and limitations. Finally, we present three case studies to demonstrate the efficacy

73   of the FloaTEM system and interpretation methodology: surveying on a shallow freshwater lake, a deep freshwater lake,

74   and in a saline bay environment.

75   **2. The FloaTEM system**

76   Operating in aquatic environments provides challenges that are unique to the setting, requiring modifications not only to

77   the instrumentation relative to land-based operation, but also to acquisition protocols and safety procedures. Navigating

78   on shallow water, lakes, or rivers, may be challenging; to assist safe navigation, real-time GPS and echo-sounder data

79   are integrated into the FloaTEM system's recording and navigation software. The echo-sounder provides the depth to the

80   river/lakebed and this information can furthermore be utilized as prior information in later data processing.

81   Design aspects of the FloaTEM system ~~depends~~depend on the application—primarily whether freshwater or saltwater—

82   and thus we have designed both a fresh water FloaTEM system (FW-FloaTEM) and a saltwater FloaTEM system (SW-

83   FloaTEM). In the following subsections, we discuss the details of freshwater and saltwater FloaTEM systems.

84   **2.1 The freshwater FloaTEM system**

85   The FW-FloaTEM has a design similar to the tTEM-system: A 4 x 2 m^2, single-turn transmitter coil (TX-coil) is followed

86   by the receiver coil (RX-coil), in a 9 m offset configuration. Figure 1 shows a schematic layout and photo of the FW-

87   FloaTEM system. The receiver coil has an effective area of 20 m^2 with a bandwidth of 420 kHz. This effective RX-area

88   is 4 times higher compared to the previously used RX-coil of the tTEM-system as described in Auken et al. (2018), and

89   therefore provides approximately a 4 times better signal to noise ratio and increased DOI (100m).

90   The fiberglass frame follows the same construction as the tTEM-system—mounted on two paddleboards instead of

91   sleds—and with additional frame components added for stability. The RX-coil is simply mounted on an inflatable rubber

92   boat. Note that all mounting and floatation devices of the TX- and RX-coils are of non-conductive materials to avoid EM

93   bias signals in the data.

94   The acquisition protocol consists of an alternating high- and low-moment transmitter pulse to obtain the sounding curve.

95   The low moment, with a peak current of ~3 A, records 15 time gates of data between 4 µs and 33 µs referenced to the

96   beginning of the turn-off of the transmitter pulse. The high-moment pulse utilizes 23 gates from 10 µs to 900 µs with a

97   peak current of ~30 A. Thanks to the latest hardware modification, the peak current is maintained with a deviation of

98   ±0.1A, which ensures a stable current waveform throughout the operation. Detailed system parameters are listed in Table-

99   1.

100   **2.2 The saltwater FloaTEM system**

101   Presence of highly conductive saltwater limits the DOI due to the slow diffusion of the eddy currents in the conductive

102   water body. In order to increase the DOI, the transmitter moment of the SW-FloaTEM is increased by a factor of eight,

103   compared to FW-FloaTEM, by doubling the transmitter loop size and increasing the number of TX-coil turns to four. The

104   saltwater configuration only utilizes a HM pulse of 25 A which is sufficient to obtain similar near surface resolution as

105   the freshwater system since the long-duration eddy currents in conductive seawater obviate the need to record very early

106   times. Further justification for using only HM is given in the synthetic studies section. Table-1 shows the parameters for

107 FW- and SW-FloaTEM systems. Observe that the last measurement gate for SW-FloaTEM is ~3 ms compared to ~1 ms
108 for FW-FloaTEM system.

109 The signal to noise ratio (S/N) is further increased by using a 40m2 RX coil. As the limiting factor for these RX coils is
110 the noise in the pre-amplifier (Nyboe and Sørensen, 2012) increasing the area of the coil increases the S/N ratio
111 proportionally. This is true as long as the area is below approximately 200 m2. Hence, the total S/N ratio increase for the
112 SW-FloaTEM system compared to the FW-FloaTEM system is a factor of 8 for the peak moment and a factor of two for
113 the RX- coil, in total a factor of 16.

114

3. Model resolution study

116 A model resolution study was conducted to investigate the influence of water depth and water conductivity on the
117 resolving capabilities of FloaTEM systems for the sub-water layers. The focus of the resolution study was the case of a
118 saltwater environment, where the conductive water layer limits the DOI significantly, and decreases the resolution of sub-
119 water resistivity structures. ~~The~~ Conclusions derived from the model resolution study ~~was also used in~~lead to the design
120 of the SW-FloaTEM system~~, and the presented results therefore include both~~. We also present the analyses of the FW-
121 ~~and~~FloaTEM system to compare against the SW-FloaTEM ~~cases~~system. The model resolution study comprises a) an
122 inversion of synthetically generated data from known layered models (the *true model*); b) a model parameter analysis of
123 the true models, and c) an estimated depth of investigation (DOI). The modelling was performed with a 1D framework,
124 and hence does not examine lateral resolution capabilities or ability to resolve 2D or 3D structures.

125 The modelling scheme consists of the following steps:

1. Calculate system-specific 1D forward data of the true model.
2. Estimate realistic data uncertainties on the forward data based on signal levels and background noise assumptions
3. ~~Estimating~~Estimate model parameter uncertainties by a computation of the model covariance matrix for the true model. (Auken et al., 2015)
4. ~~Performing 1D smooth inversions of the forward data including DOI estimates.~~ Perform 1D smooth inversions of the forward data including DOI estimates (Christiansen Vest and Auken, 2012).

132 All the modellings were carried out with the AarhusInv modelling code (Auken et al., 2015). The FW- and SW-FloaTEM
133 systems were modelled as described in Table 1. The data uncertainty was model dependent, based on a background noise
134 level at $1nV/m^2$ at 1 ms plus a uniform contribution of 3%. The uniform uncertainty is the main contribution to data
135 uncertainty due to the relatively conductive models producing high signals. For the model parameter analysis, a priori
136 constraints on the water column were applied with a 10% uncertainty for the water depth and a 30% uncertainty for the
137 resistivity of the water. For the inversion, no lateral constraints were applied. However, for the model parameter analysis
138 lateral constraints were assumed between 5 similar neighboring models (based on the true model) to simulate the improved
139 resolution capabilities from information sharing when working with field data. For the inversion of the forward data, a
140 smooth 30-layer model description was used with logarithmic increasing layer thicknesses with depth, and with an
141 additional top layer representing the depth and resistivity of the water column. All inversions were carried out using a
142 homogenous starting resistivity model.

143 Two model sweeps were constructed, each consisting of 15 three-layer models (True models). In model sweep 1 (Fig.
144 2a), the thickness (water depth) was varied of a 0.3 Ωm top layer from one to 15 m. In model sweep 2 (Fig. 3a) the
145 resistivity of a 7 m thick water layer was varied from 0.1 - 3 Ωm. In both model sweeps, the second layer was 3 Ωm
146 / 10 m thick, and the third layer 30 Ωm.

147 The modeling results for model sweep 1 are shown in Fig. 2. Since the modeling was carried out in log-model space, the
148 model parameter analysis (Fig. 2b and 2c) shows the relative uncertainties estimates (STD-factor) of the model
149 parameters. In general, a model parameter (resistivity or thickness) will be considered resolved if the STD-factor is less
150 than 1.5, moderately resolved if between 1.5-2.0 and unresolved if greater than 2. From the model parameter analysis in
151 Fig. 2b and 2c, we observe, as expected, that the resolution of the model in general decreases with increasing water depth.
152 The water layer is very well resolved in all cases partly because of the prior constraints and partly due to the method's
153 high sensitivity to the conductive water layer. In the SW-FloaTEM case (Fig. 2b) the resistivity of the second layer is
154 resolved (STD-factor < 2) to a water depth of about 7 m and the layer boundary between layer two and three (DEP 2) is
155 resolved to a water depth of about 10 m. In the FW-FloaTEM case the (Fig. 2c) the resistivity of the second layer is
156 resolved (STD-factor < 2) to a water depth of about 5 m and the layer boundary to a water depth of only around 4 m.
157 Also, for the third layer, the resistivity was better resolved in the SW-FloaTEM system case than in the FW case.

158 The inversion results of the true model data, with DOI estimates in Fig. 2d and 2e, are in-line with the observations from
159 the model parameter analysis. Increasing water depth results in a shallower DOI and loss of resolution of the sub-water
160 layers, and the SW-FloaTEM system performs better than the FW-FloaTEM system.

161 Water depth is not the only parameter of importance for the resolution capabilities, but also the resistivity or conductivity
162 of the water. Figure 3 shows the modeling results for model sweep 2 with a varying resistivity of a 7 m thick water layer.
163 For a very conductive water layer of 0.1-0.2 Ωm, the resolution is limited for both systems, as observed in the model
164 parameter analysis as well as in the inversion sections of Fig. 3. When the water resistivity is above 0.3-0.4 Ωm, the
165 SW system resolves/recovers the sub-water layers very well (Fig. 3b and 3d). Especially in resolving the boundary
166 between second and third layer (DEP2), the SW-system performs much better than the FW-system, which is also clearly
167 reflected in the DOI of the two systems.

168 Based on the presented analysis and other analyses (not shown in this paper), we conclude that the conductance (product
169 of conductivity and thickness) of the water column should be below approximately 25 Siemens for this particular SW-
170 FloaTEM system to able to penetrate the water column and map sub-water layers. It was also clear that the S/N ratio for
171 the SW system had to be increased significantly compared to the FW system, but the very early time gates were not
172 needed, and a slower turn-off and lower bandwidth of the RX-coil was acceptable. This led to the compromise of more
173 turns in the transmitter coil, only high moment cycles and the larger area of the RX-coil.

174 **4. Field cases**
175 We present three surveys conducted with the FloaTEM system in Denmark: Two on freshwater lakes, and one on seawater
176 in a fjord. These datasets represent different water conductivities and various glacial sediment settings. Details of
177 processing and inversion of FloaTEM data are given in appendix-A. Some of the cases needed special handling of the

178 inversion process and this is described in the respective case study section. Table 2 summarizes key survey conditions
179 and modeling parameters.

4.1 Freshwater cases

181 We present two freshwater cases from two lakes in central Jutland, Denmark, to demonstrate the utility of the FloaTEM-
182 FW system in a shallow and a deep lake scenario.

4.1.1 Lake Sunds

184 Lake Sunds spans 127 hectares and is quite shallow (1.5 m - 2.5 m) with a maximum depth of 4.5 m. It is sitting in a late
185 Weichselian meltwater plain. The City of Sunds has developed around the lake, and the majority of the ~4000 inhabitants
186 of Sunds live close to the water. In recent years the groundwater table in Sunds has risen substantially, which causes
187 problems in the winter period where the groundwater is the highest and periods of heavy rain then results in flooded
188 cellars in residential houses. The problem is exacerbated by an old sewage system in the city with many worn pipes. These
189 pipes are under replacement, but this will remove the current drainage by worn pipes, and the consequences would be a
190 further rise of the groundwater table. On top of the flooding of cellars, there is a risk that the groundwater fluctuations
191 can mobilize near-surface pollutants from otherwise hydrologically inactive point-source pollutions in the city such as
192 old gas stations and landfills and hence contaminate the groundwater in the area.

193 From a hydrogeological viewpoint the shallow water table has puzzled the water managers as shallow boreholes from the
194 area show that the geology in the upper 20 meters is pure sand as expected in a meltwater plain environment. It was
195 therefore decided to setup a detailed groundwater model to investigate groundwater flow paths and identify measures to
196 control the groundwater table fluctuations.

197 The area to the east of the lake has been mapped with tTEM, covering a total of 816 hectares, with a FloaTEM survey
198 subsequently performed on the lake (Fig. 4). Additionally, multiple boreholes provide lithological data for comparison,
199 although the majority of the boreholes only reach 10-20 meters depth. Most of them were drilled in the 1940's in
200 connection to brown-coal mapping.

201 The tTEM and FloaTEM data were inverted separately, with the results combined in Figure 5. Profile A in Fig. 4 is
202 entirely on the lake and profile B is oriented north-south crossing the lake. In profile A, FloaTEM inversion results
203 generally show a good agreement with the available borehole description (B1 and B2) which is broadly categorized as
204 sand, clay and silt containing organic material. However, there is a slight mismatch between lithological boundaries
205 observed in some boreholes and inversion models. This mismatch may be caused by borehole offset from FloaTEM
206 profiles, possibly exaggerated by erroneous location data for the more than 70-years-old logs. The distance of Borehole
207 B1 and B2 from the profile are 20 and 25m. Overall, the resistivity model indicates a presence of two areas with a thick
208 organic silt layer below the water column (Fig. 5a and 5c) followed by a thick and more resistive sand layer. The sand
209 layer thins out towards the bank of the lake and appears to go to the surface outside the lake as indicated in profile B. The
210 information about thickness and location of the organic silts are of great importance in the groundwater model of the area,
211 since these old lake deposits are impermeable and thereby guide groundwater flow beneath the lake.

212 Figure 5c-f shows mean resistivity maps at four depth intervals and includes both the FloaTEM and the tTEM survey
213 results. The mean resistivity maps indicate that there is a large degree of spatial variability of sediment types in and around

214 Lake Sunds. The heterogeneity beneath the lake would not be possible to resolve by interpolating across; this
215 heterogeneity is related to the lake genesis and reveals where the water table beneath the town of Sunds is in hydrologic
216 contact with the lake. Furthermore, the tTEM and FloaTEM results show that the geological setting is not a simple
217 sandbox at depth. At 20 meters depth and below we have several Tertiary clay layers with a resistivity of 10-30 ohm-m,
218 which have been deformed by glaciers and glacial tectonics. The information about the clay layers is crucial for the deeper
219 parts of the groundwater model.

4.1.2 Lake Ravn

221 Lake Ravn is located in Eastern Jutland, Denmark. It is the second deepest lake in Denmark with depths generally ranging
222 from 25 to 30 m, and with a maximum depth of 34 m. The lake was formed as a dead-ice hole located on top of a WSW-
223 ENE oriented partly-buried valley (Sandersen, 2016).

224 In the rOpen project (https://hgg.au.dk/projects/ropen), the Javngyde watershed northwest of Lake Ravn was mapped in
225 detail with tTEM, and it was modelled with a 3D finite difference groundwater flow model. The purpose of the rOpen
226 project was to estimate the total amount of nitrate reduction along flow pathways from the water table to a surface water
227 recipient. The rOpen work and a related hydrological modelling study (Rumph Frederiksen and Molina-Navarro, 2021)
228 revealed that around 40% of the infiltrating water crossed the surface watershed as groundwater flow to Lake Ravn.
229 However, the hydraulic connectivity between the watershed and the lake was poorly understood, and it was decided to
230 perform a FloaTEM survey on the lake to obtain more information about the hydrological system.

231 The survey was conducted with east/west oriented lines with a spacing of 60 m combined with lines encompassing the
232 perimeter of the lake (Fig. 6). Only electric boat engines are allowed on the lake, limiting the acquisition speed to 6 km/h.
233 Strong winds on the day of acquisition further challenged the navigation and resulting in head-wind lines being wigglier
234 than the tail-wind lines.

235 The resistivity model for Lake Ravn (Figure 7) shows multiple features of interest. The relatively high resistivity of the
236 lake water has allowed for extended depths of investigation, despite the deep-water column. The resistivity models have
237 a DOI down to 90 m below the lake surface. Within the water column we see resistivity changes, and this is verified by
238 direct current resistivity measurements conducted in 0.5 m depth intervals at multiple locations (not shown). The water
239 resistivity measurements were conducted using a 10 cm Wenner configuration. The measured resistivity of the water
240 column gradually varies from the top to the bottom of the lake, from ~27 to ~34 Ωm probably due to temperature
241 variations. For this reason, the water column was modeled with two resistivity layers with a priori constrained resistivity
242 values and a constrained water depth (depth to bottom of 2nd water layer), but with a free interface between the two water
243 layers. Beneath the bottom of the lake (Profile AA' and BB' in Fig. 6), we observe sandy layers, underlain by a clay layer
244 interpreted to be Oligocene. Below the bottom of the lake, we observe a thin conductive layer which is interpreted as fine
245 sediments deposits such as clay or silt. The mean resistivity maps (Fig. 7c-f) at different depths reveal a large
246 heterogeneity in the geology below Lake Ravn. Along the shore of the lake, we observe sandy deposits, which most likely
247 play an important role in discharging groundwater to the lake.

4.2 Saltwater study

Horsens bay is a shallow fjord located in the western Baltic sea, Denmark, roughly 18 km long and 2-3 km wide. It has poor ecological status, possibly due to submarine groundwater discharge causing excessive loading of nutrients (Hinsby et al., 2012). Increased loading of nutrients has caused the Baltic sea ~~as~~to be one of the most polluted seas in the world (Pihlainen et al., 2020; Meier et al., 2019). To understand the vulnerability of the Horsens Fjord and coastal zone dynamics an improved understanding of land-sea interactions including contaminant pathways in the subsurface, in relation to nutrient and salinity variations, is needed.

The water depth within the survey area (Fig. 8) ranges from 2 m (minimum water depth for safe maneuverability with the specific vessel) to 8 m in the central area. FloaTEM data were acquired in North-South striking lines across the bay (Figure 8), with a line spacing of ~25 m and an operational speed of 12-14 km/h. The relatively small survey was conducted in collaboration with the Geological Survey of Denmark and Greenland (GEUS). The purpose was to identify and map fresh groundwater flow into the fjord, which may provide pathways for nitrate leaching from the surrounding farmland into the bay. The geology beneath the Horsens fjord includes quaternary meltwater sand and gravel constituting as aquifer and quaternary clay tills and Miocene mica clay as aquitards (Jørgensen et al., 2010). A narrow channel connects the fjord to deeper waters in the Baltic Sea. The central part of the fjord is dominated by muddy sediments due to the high accumulation of organic material. Till deposits are present in shallow coastal areas.

FloaTEM inversion results are presented in Fig. 9. The resistivity model in Horsens Bay (profile A in Figure 9) constitutes a three-layer model where the top layer is the sea water followed by a conductive clay-rich infill sediments, likely an extension of the Tørring/Horsens valley (Sandersen, 2016). The sequence is generally fining-upward, with significant imprints of paleo-topography. Below the clay-rich layer, a third layer with elevated resistivity is present; interpreted as a meltwater sand unit but saturated with sea water. The resistivity of this sand unit appears to be low (10-15 ohm-m) compared to one would expect for fresh water saturated sand. This sandy unit is most likely leading the groundwater discharge into the seabed at locations where the overlaying clay-till unit is sufficiently thin.

The mean resistivity maps (Fig. 9 b-e) show the spatial variability of the clay-till and sand rich sediments at four depth intervals below the sea water label. We see that the sediment close to the coast has a higher resistivity than what is observed in the middle of the fjord. This might be a transition from a sandy sediment towards a more clay-rich environment in the middle of the fjord. The knowledge of extension of these sand rich sediments from coast to the middle of fjord, helps us to locate the probable regions where groundwater may discharge into fjord. Additionally, we also observe a small, northwest trending low resistivity structure indicates a paleo-channel, which has been confirmed by shallow-seismic data (not shown).

5. Discussion

The resistivity of a surface water body can change over short distances, so inversions will often benefit from a spatially varying resistivity constraint or reference. The need for a priori water resistivity and depth is higher in the freshwater cases than the saltwater case. The high conductivity in saltwater environments usually results in a well-resolved water column, so a priori information is less important. While the current instrument is integrated with a depth sounder, it is not difficult to fit it with a conductivity logger as well to supply relevant a priori values for the water column. We note that the choice in towing vessel is important as a larger vessel requires a longer towing distance.

In general, the data quality for FloaTEM is usually better than comparable land surveys as lakes and rivers are often far from interfering infrastructure, which means that a FloaTEM survey normally results in full data coverage without gaps from data culling.

FloaTEM data provide critical information regarding sub-lake or sub-sea geology. In the Lake Sunds example, an interpretation based on land data only with lithological boundaries interpolated across the lake would be quite erroneous by missing the unique features associated with the genesis of the lake. The FloaTEM system provides a means of capturing these features which would be infeasible to identify with boreholes.

The depth of investigation is highly dependent on not only the resistivities of soils, but also of the conductivity of the waters as the synthetic modeling study showed, where even a small conductivity change in the saltwater can reduce the DOI significantly. This stresses that a priori information about water salinity values is critical in selecting between the FW-FloaTEM and SW-FloaTEM configurations and designing the particular survey design.

The high signal level in conductive saltwater environments often results in very low noise, also at the latest recorded time gate at ~2 ms. In these cases, increasing the recording time and reducing the repetition rate should increase the DOI by adding more late-time data. However, a lower repetition rate may also lead to higher motion induced noise in the receiver coil, which can become the dominating noise for the late time gates.

The results showed here all focused on delineation of hydrological permeable (sands) and impermeable (clays) lithologies in the context of improving large-scale hydrological understanding and prediction strength. Though, from the given examples it should be clear that the application range of FloaTEM spans much more. A few examples include foundation investigations for offshore wind farms; raw material exploration beneath lakes and rivers; and geotechnical pre-investigations for cabling routes below water bodies.

6. Conclusions

We have developed a new towed, easily configurable floating TEM instrument, FloaTEM, and successfully applied the system to both freshwater and saltwater studies to investigate geology and hydrology beneath lakes and shallow seawater. The FloaTEM system is modular, so longer beams can be used to increase the transmitter moment and likewise more transmitter turns can be added, both increasing the depth of investigation. Supported by synthetic analysis, we reconfigured a freshwater FloaTEM system to a saltwater FloaTEM system, primarily by increasing the transmitter moment and decreasing the noise in the receiver coil enabling us to perform FloaTEM surveys not only on both shallow and deep lakes, but also on shallow saltwater up to 8 meters deep.

The conductance of the water, water depth multiplied with water conductivity, is the limiting factor when surveying on saline water. Based on the presented analysis the water column should be below ~25 Siemens for the system to penetrate the water column and map sub-water layers. For freshwater lakes and rivers, depths of investigation of 80 meters or more are possible, while in saltwater cases we can achieve depths of investigation of 10-25 meters strongly depending on water depth and conductivity.

With the FloaTEM system, we can map geological layers beneath the water bodies, normally not accessible for mapping with ground based geophysical methods, thereby allowing for detailed hydrological modelling in these often-important

areas as well. Through 2 freshwater cases and one saltwater case we show the system's ability to image the heterogeneous

geology beneath water bodies. In the freshwater cases the FloaTEM datasets revealed geological information that would

have been impossible to deduce from land-based-only information and in the saltwater case the data delivered clear images

on the clay-sand distribution beneath the seafloor.

7. Author contribution

PM design and develop methodology, instrumentation, data processing and inversion, wrote the first draft of manuscript.

FC carried out data collection, data analyses and contributed to original manuscript. JP and MK contributed to first draft

of the manuscript and interpretations and feedback on inversion results. RF provided data interpretations, feedback and

contributed to the writing of original manuscript. NF carried out synthetic data analysis and field data inversion of Ravnsø

lake. AV and EA conceptualized the methodology, contributed to writing original manuscript and provided feedback.

8. Acknowledgements

We thank TOPSOIL, an Interreg project supported by the North Sea Programme of the European Regional Development

Fund of the European Union, and the development has been funded by Innovation Fund Denmark, project rOpen (Open

landscape nitrate retention mapping) and MapField (Field-scale mapping for targeted N-regulation), WATEC (Aarhus

university Centre for water technology) and internal HGG (Hydrogeophysics group at Arhus university) funding. Partial

support for data collection and interpretation of results were provided by GEUS (Geological survey of Demark and

Greenland).

References

Auken, E., Jørgensen, F., and Sørensen, K. I.: Large-scale TEM investigation for groundwater, Exploration Geophysics, 33, 188-194, 2003.

Auken, E., Christiansen, A. V., Westergaard, J. A., Kirkegaard, C., Foged, N., and Viezzoli, A.: An integrated processing scheme for high-resolution airborne electromagnetic surveys, the SkyTEM system, Exploration Geophysics, 40, 184-192, 2009.

Auken, E., Foged, N., Larsen, J., Lassen, K., Maurya, P., Dath, S., and Eiskjær, T.: tTEM — A towed transient electromagnetic system for detailed 3D imaging of the top 70 m of the subsurface, GEOPHYSICS, E13-E22, 10.1190/geo2018-0355.1, 2018.

Auken, E., Christiansen, A. V., Fiandaca, G., Schamper, C., Behroozmand, A. A., Binley, A., Nielsen, E., Effersø, F., Christensen, N. B., Sørensen, K. I., Foged, N., and Vignoli, G.: An overview of a highly versatile forward and stable inverse algorithm for airborne, ground-based and borehole electromagnetic and electric data, Exploration Geophysics, 2015, 223-235, 2015.

Barker, R. D.: Applications of geophysics in groundwater investigations, Water Services, 84, 1980.

Binley, A. and Kemna, A.: DC Resistivity and Induced Polarization Methods, in: Hydrogeophysics, edited by: Rubin, Y., and Hubbard, S. S., Springer Netherlands, Dordrecht, 129-156, 10.1007/1-4020-3102-5_5, 2005.

Briggs, M. A., Nelson, N., Gardner, P., Solomon, D. K., Terry, N., and Lane, J. W.: Wetland-Scale Mapping of Preferential Fresh Groundwater Discharge to the Colorado River, 57, 737-748, https://doi.org/10.1111/gwat.12866, 2019.

Christiansen, A. V., Auken, E., and Sørensen, K. I.: The transient electromagnetic method, in: Groundwater Geophysics. A tool for hydrogeology, 1 ed., edited by: Kirsch, R., Springer, 179-224, 2006.

Christiansen vest, A. and Auken, E.: A global measure for depth of investigation, Geophysics, 77, WB171-WB177, 2012.

Danielsen, J. E., Auken, E., Jørgensen, F., Søndergaard, V., and Sørensen, K. I. J. J. o. a. g.: The application of the transient electromagnetic method in hydrogeophysical surveys, 53, 181-198, 2003.

Day-Lewis, F. D., White, E. A., Johnson, C. D., Lane, J. W., and Belaval, M.: Continuous resistivity profiling to delineate submarine groundwater discharge—examples and limitations, The Leading Edge, 25, 724-728, 10.1190/1.2210056, 2006.

Dickey, K. A.: Geophysical investigation of the Yellowstone Hydrothermal System, Geophysics, Virginia Tech, 110 pp., 2018.

Fitterman, D. V. and Deszcz-Pan, M.: Helicopter EM mapping of saltwater intrusion in Everglades National Park, Florida, Exploration Geophysics, 29, 240-243, 10.1071/EG998240, 1998.

Gustafson, C., Key, K., and Evans, R. L.: Aquifer systems extending far offshore on the US Atlantic margin, Scientific Reports, 9, 1-10, 2019.

Harvey, J. and Gooseff, M.: River corridor science: Hydrologic exchange and ecological consequences from bedforms to basins, 51, 6893-6922, https://doi.org/10.1002/2015WR017617, 2015.

Hatch, M., Munday, T., and Heinson, G.: A comparative study of in-river geophysical techniques to define variations in riverbed salt load and aid managing river salinization, 75, WA135-WA147, 10.1190/1.3475706, 2010a.

Hatch, M., Munday, T., and Heinson, G.: A comparative study of in-river geophysical techniques to define variations in riverbed salt load and aid managing river salinization, Geophysics, 75, WA135-WA147, 2010b.

Hinsby, K., Markager, S., Kronvang, B., Windolf, J., Sonnenborg, T., and Thorling, L.: Threshold values and management options for nutrients in a catchment of a temperate estuary with poor ecological status, Hydrology and Earth System Sciences, 16, 2663-2683, 2012.

Jørgensen, F., Møller, R. R., Sandersen, P. B., and Nebel, L.: 3-D geological modelling of the Egebjerg area, Denmark, based on hydrogeophysical data, GEUS Bulletin, 20, 27-30, 2010.

Kwon, H.-S., Kim, J.-H., Ahn, H.-Y., Yoon, J.-S., Kim, K.-S., Jung, C.-K., Lee, S.-B., and Uchida, T. J. E. G.: Delineation of a fault zone beneath a riverbed by an electrical resistivity survey using a floating streamer cable, 36, 50-58, 2005.

Lane, J. W., Briggs, M. A., Maurya, P. K., White, E. A., Pedersen, J. B., Auken, E., Terry, N., Minsley, B., Kress, W., LeBlanc, D. R., Adams, R., and Johnson, C. D.: Characterizing the diverse hydrogeology underlying rivers and estuaries using new floating transient electromagnetic methodology, Science of The Total Environment, 740, 140074, https://doi.org/10.1016/j.scitotenv.2020.140074, 2020.

Manheim, F. T., Krantz, D. E., and Bratton, J. F.: Studying Ground Water Under Delmarva Coastal Bays Using Electrical Resistivity, 42, 1052-1068, https://doi.org/10.1111/j.1745-6584.2004.tb02643.x, 2004.

Maurya, P. K., Christiansen, A. V., Pedersen, J. B., and Auken, E.: High resolution 3D subsurface mapping using a towed transient electromagnetic system - tTEM: case studies, Near Surface Geophysics, 18, 16, 10.1002/nsg.12094, 2020.

Meier, H., Edman, M., Eilola, K., Placke, M., Neumann, T., Andersson, H. C., Brunnabend, S.-E., Dieterich, C., Frauen, C., and Friedland, R.: Assessment of uncertainties in scenario simulations of biogeochemical cycles in the Baltic Sea, Frontiers in Marine Science, 6, 46, 2019.

Micallef, A., Person, M., Haroon, A., Weymer, B. A., Jegen, M., Schwalenberg, K., Faghih, Z., Duan, S., Cohen, D., and Mountjoy, J. J.: 3D characterisation and quantification of an offshore freshened groundwater system in the Canterbury Bight, Nature Communications, 11, 1-15, 2020.

Minsley, B. J., Rigby, J. R., James, S. R., Burton, B. L., Knierim, K. J., Pace, M. D. M., Bedrosian, P. A., and Kress, W. H.: Airborne geophysical surveys of the lower Mississippi Valley demonstrate system-scale mapping of subsurface architecture, Communications Earth & Environment, 2, 131, 10.1038/s43247-021-00200-z, 2021.

Mollidor, L., Tezkan, B., Bergers, R., and Löhken, J.: Float-transient electromagnetic method: in-loop transient electromagnetic measurements on Lake Holzmaar, Germany, Geophysical Prospecting, 61, 1056-1064, 10.1111/1365-2478.12025, 2013.

410 Munk, L., Hynek, S., Bradley, D. C., Boutt, D., Labay, K. A., and Jochens, H.: Lithium brines: A global
411   perspective: Chapter 14, 2016.
412 Nyboe, N. S. and Sørensen, K. I.: Noise reduction in TEM: Presenting a bandwidth- and sensitivity-optimized
413   parallel recording setup and methods for adaptive synchronous detection, Geophysics, 77, E203-
414   E212, 2012.
415 Ong, J. B., Lane, J. W., Zlotnik, V. A., Halihan, T., and White, E. A.: Combined use of frequency-domain
416   electromagnetic and electrical resistivity surveys to delineate near-lake groundwater flow in the
417   semi-arid Nebraska Sand Hills, USA, Hydrogeology Journal, 18, 1539-1545, 10.1007/s10040-010-
418   0617-x, 2010.
419 Parsekian, A. D., Singha, K., Minsley, B. J., Holbrook, W. S., and Slater, L.: Multiscale geophysical imaging of
420   the critical zone, 53, 1-26, https://doi.org/10.1002/2014RG000465, 2015.
421 Pihlainen, S., Zandersen, M., Hyytiäinen, K., Andersen, H. E., Bartosova, A., Gustafsson, B., Jabloun, M.,
422   McCrackin, M., Meier, H. M., and Olesen, J. E.: Impacts of changing society and climate on nutrient
423   loading to the Baltic Sea, Science of the Total Environment, 731, 138935, 2020.
424 Rey, D. M., Walvoord, M. A., Minsley, B., Rover, J., and Singha, K.: Investigating lake-area dynamics across a
425   permafrost-thaw spectrum using airborne electromagnetic surveys and remote sensing time-series
426   data in Yukon Flats, Alaska, Environmental Research Letters, 14, 025001, 10.1088/1748-9326/aaf06f,
427   2019.
428 Rumph Frederiksen, R. and Molina-Navarro, E.: The importance of subsurface drainage on model
429   performance and water balance in an agricultural catchment using SWAT and SWAT-MODFLOW,
430   Agricultural Water Management, 255, 107058, https://doi.org/10.1016/j.agwat.2021.107058, 2021.
431 Sandersen, J. F.: Kortlægning af begravede dale i Danmark. Opdatering 2015. GEUS Særudgivelse.,
432   http://begravededale.dk/PDF_2015/091116_Rapport_Begravede_dale_BIND_1_Endelig_udgave.p
433   df, 2016.
434 Sheets, R. and Dumouchelle, D.: Geophysical Investigation Along the Great Miami River From New Miami to
435   Charles M. Bolton Well Field, Cincinnati, Ohio, U. S. Geological Survey, 2009.
436 Siemon, B., Christiansen, A. V., and Auken, E.: A review of helicopter-borne electromagnetic methods for
437   groundwater exploration, Near Surface Geophysics, 7, 629-646, 2009.
438 Sophocleous, M.: Interactions between groundwater and surface water: the state of the science,
439   Hydrogeology journal, 10, 52-67, 2002.
440 Viezzoli, A., Auken, E., and Munday, T.: Spatially constrained inversion for quasi 3D modelling of airborne
441   electromagnetic data - an application for environmental assessment in the Lower Murray Region of
442   South Australia, Exploration Geophysics, 40, 173-183, 2009.
443 Winter, T. C., Harvey, J. W., Franke, O. L., and Alley, W. M.: Ground Water and Surface Water A Single
444   Resource1139, 1998.

445 **List of Figures**

446
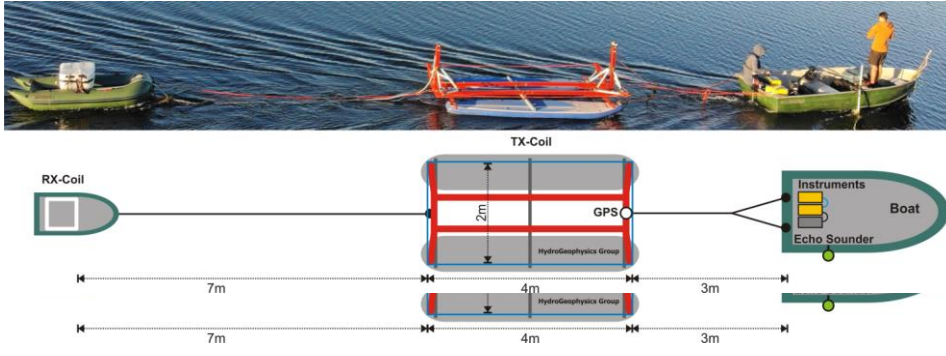
447

448 **Figure 1: Picture and schematic of the freshwater FloaTEM configuration, with boat, transmitter coil (TX-coil), and receiver**
449 **coil (RX-coil). In contrast, the saltwater configuration uses a 4m x 4m transmitter coil.**

450
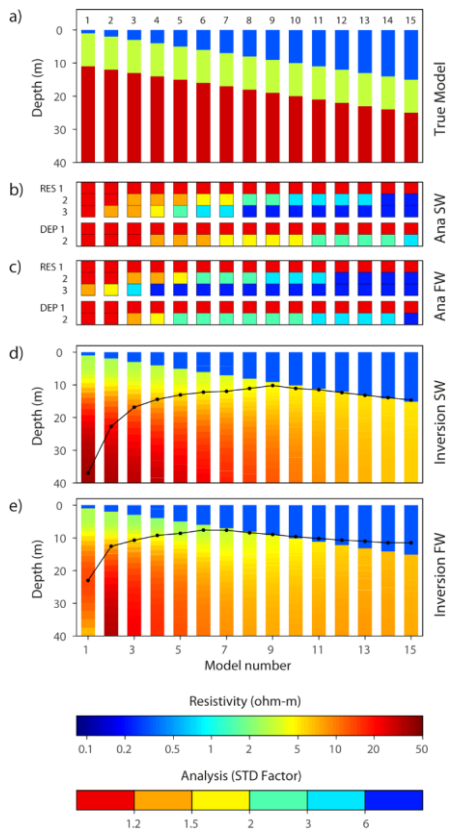
Figure 2. a) True model. Number on top of each model bar states the water depth (thickness of first layer). b-c) Model parameter
analyses of the true models, stated as a standard deviation factor, for the SW- and FW-FloaTEM systems. d-e) Inversion results
for SW- and FW-FloaTEM systems. The black line shows the DOI.

454
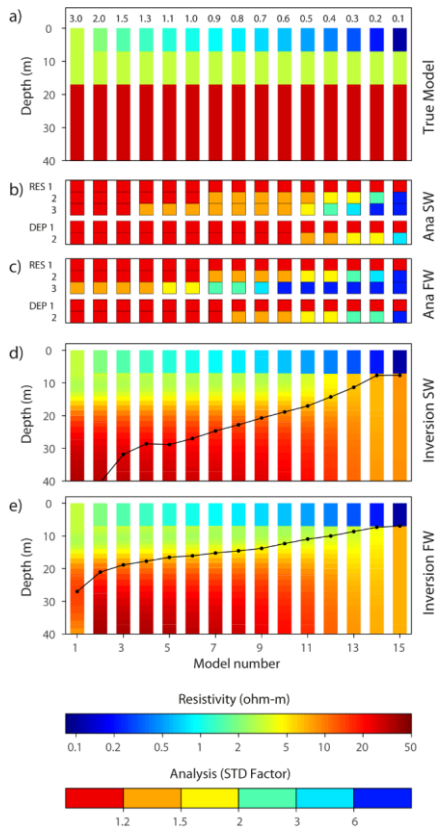
Figure 3. Model sweep 2. a) True model. Number on top of each model bar states the resistivity of the water (resistivity of first layer). b-c) Model parameter analysis of the true model, stated as standard deviation factor, for the SW- and FW-FloaTEM systems. d-e) Inversion results for SW- and FW-FloaTEM systems. The black line shows the DOI.

458
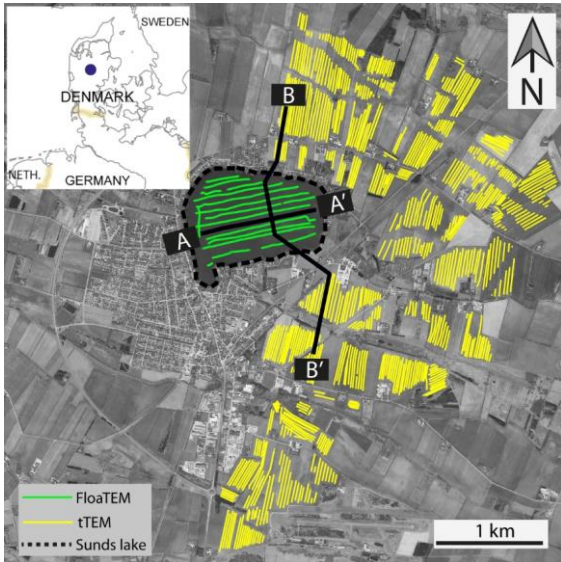
Figure 4 Sunds FloaTEM and tTEM survey region with FloaTEM lines marked in green and tTEM in yellow. AA' and BB'
are the profiles that are presented in Figure 5.

462
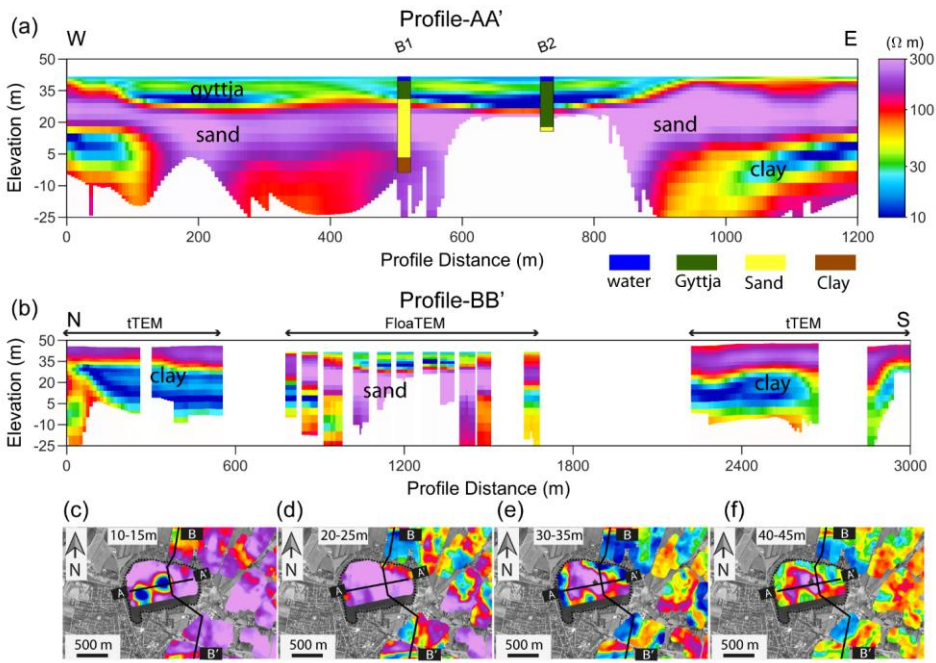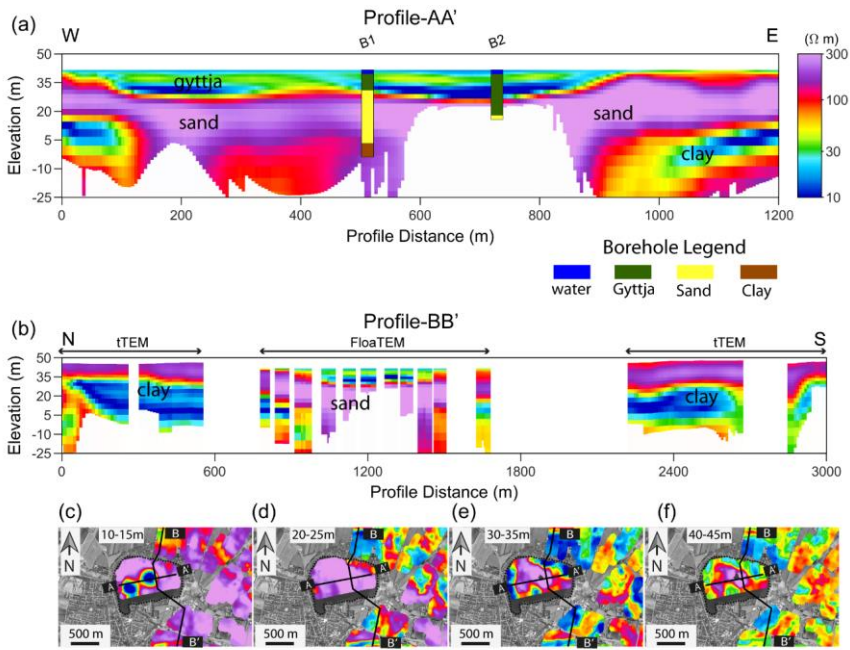
Figure 5: Results from Sunds joint tTEM and FloaTEM survey. Location of profile AA' and BB' is marked in ~~Error! Reference source not found.~~**figure 4**Error! Reference source not found.**; note that while the elevation axis is identical, the profiles have different lengths and thereby different vertical exaggeration. Profile-AA' includes lithological interpretations from available boreholes near the survey line. Note that the water column is included in the figure, but only 2 meters thick, (c) - (f) show mean-resistivity maps at various depth intervals with profile -AA' and BB' indicated as solid black line. Lake Sunds is marked with dotted black line.**

469
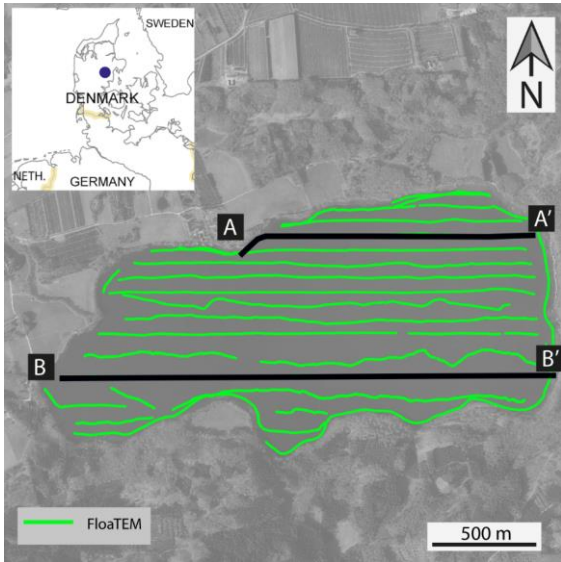
Figure 6: Survey region for the Lake Ravn FloaTEM survey. Locations of the profiles in Figure 7 are highlighted as solid
black lines

472
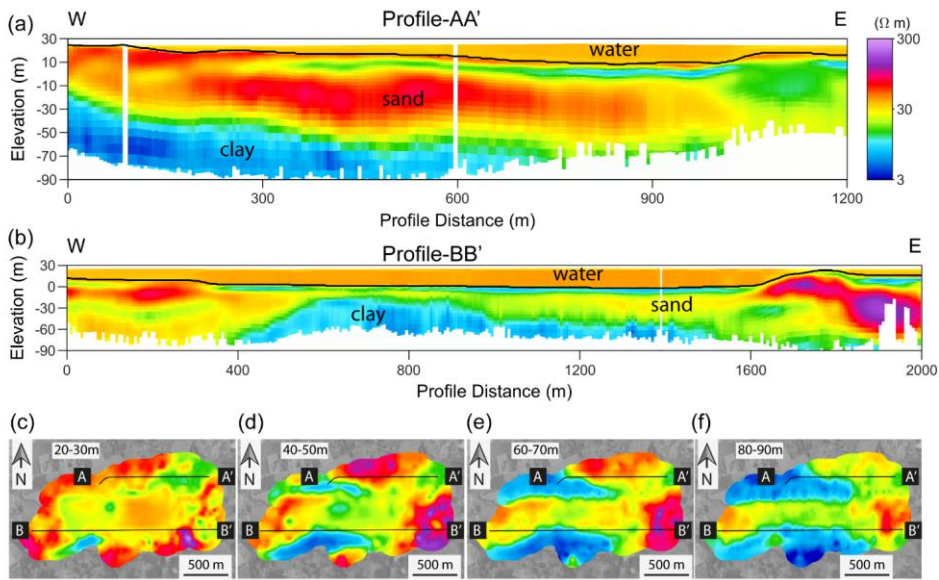
Figure 7: Results from Lake Ravn FloaTEM survey. Location of the resistivity sections AA' and BB' are marked in ~~Error! Reference source not found.~~Error! Reference source not found.**. The black line in the sections marks the lake bottom while the white faded colors indicate the DOI. (c) – (f) show mean-resistivity maps at 4 depth intervals below surface together with location of profile AA' and BB'.**
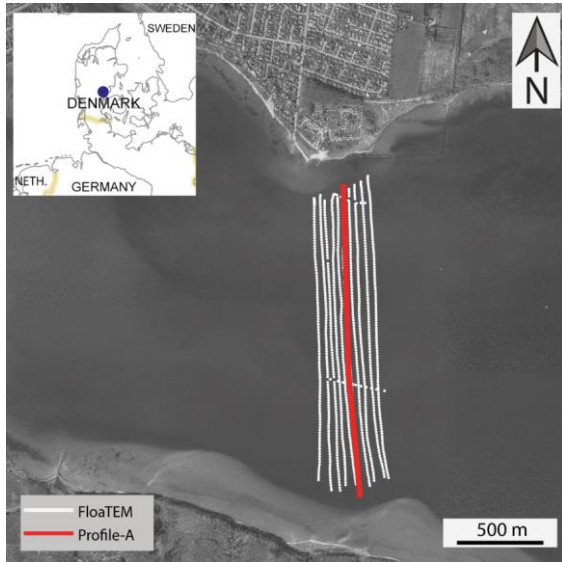
477

478 **Figure 8: Horsens Bay with FloaTEM survey lines. The red highlighted profile marks the location of the resistivity section**
479 **showed in figure. 9**

480
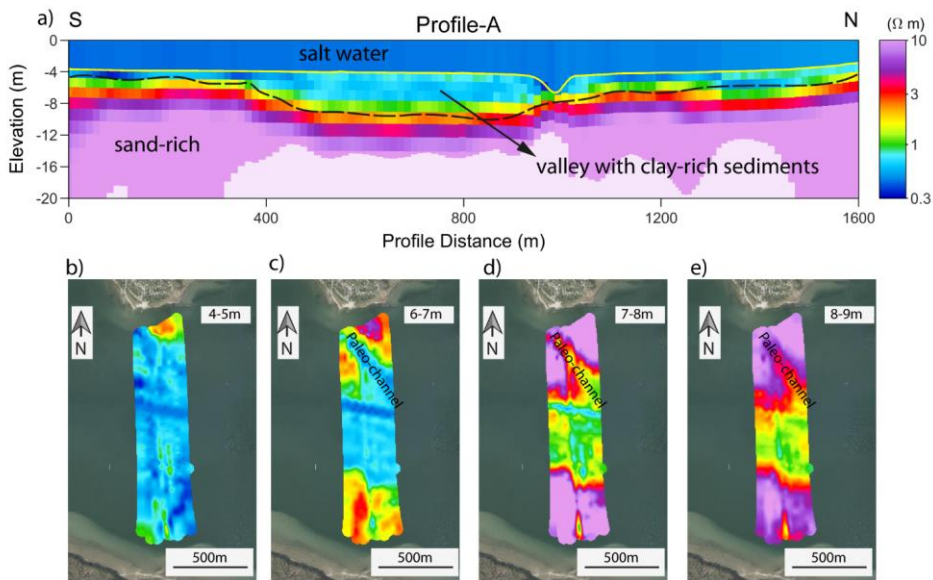
Figure 9: Resistivity mapping results from Horsens Bay. (A) Resistivity section (location marked in Figure 8) with the seafloor marked with the yellow line. (b-e) Mean resistivity maps at different depths.

List of Tables

FloaTEM system	FW-FloaTEM		SW-FloaTEM
	Low moment	High moment	High moment
Transmitter area	8 m^2		16 m^2
Number of turns	1		4
TX peak current	~3 A	~30 A	~25 A
TX peak moment	~24 Am^2	~240 Am^2	1600 Am^2
Repetition frequency @ 50 Hz power line frequency	2110 Hz	630 Hz	220 Hz
Duty cycle	42%	30%	22%
Tx on-time	200 µs	450µs	1000 µs
Turn-off time	2.6 µs	4.5 µs	14.10 µs
Gate time interval (from beginning of turn-off)	4-33 µs	10-900 µs	20-2800 µs
RX coil area	20 m^2	20 m^2	40 ~~mm^2~~
RX coil bandwidth	420 kHz	420 kHz	140 k Hz
Number of gates	15	23	26

Table 1: System parameters for the freshwater and saltwater FloaTEM systems.

Survey area	Max. water depth	System	Line spacing nominal	Water depth prior constraint	Water resistivity, prior constraint
Lake Sunds	4.5 m	FW-FloaTEM	50 m	1.03	15 ΩΩm, None
Lake Ravn	34 m	FW-FloaTEM	60 m	1.05	*28 ΩΩm, 1.1 *34 ΩΩm, 1.05
Horsens fjord	8 m	SW-FloaTEM	35 m	1.05	0.3 ΩΩm, None

489

Table 2: Survey configurations and conditions of the three case areas. The * indicates that the water column was modeled with two resistivity layers.

492

Appendix-A

Data processing and inversion

In this section, we give an overview of the data processing and inversion scheme used for FloaTEM data. In each of the case studies, FloaTEM data were processed with the Aarhus Workbench software from Aarhus GeoSoftware (www.arhusgeosoftware.dk). The standard FloaTEM processing flow follows Auken et al. (2009). Raw db/dt data are first processed to remove coherent coupling interference due to nearby infrastructures and then stacked to produce soundings with approximately 10 m spacing. In the presented cases, a short smoothing filter was applied on the recorded water depth data, but this step depends on the quality of the depth sounder data at hand. A preliminary inversion is then performed to evaluate and adjust the first-step processing of raw db/dt data.

The final inversions of the FloaTEM data were carried out using a spatially constrained inversion formulation, SCI (Viezzoli et al., 2009) using a 30–layer smooth model with layer thicknesses of layers 2-30 increasing logarithmically down to 120 m. The thickness of layer 1 is set to the water depth with a ~~fairly~~ tight prior constraint. No vertical resistivity constraints are applied from the water layer (layer 1) to the sub-layers (layers 2-30), hereby allowing a shape boundary at the lake-/ seabed in the inversion results. The water depth prior information can be taken from the echo-sounder data or from an external bathymetry grid. Additionally, prior constraints can be added to the resistivity of the water layer if separate measurement of the water conductivity are present. In some cases, it is insufficient to model the water column as one homogeneous layer, e.g.~~.,~~ probably due to a halocline or thermocline. In these cases, more layers are introduced to represent the water column in the inversion setup and the prior water depth is assigned to the depth to the bottom of the last water layer.

Figure A1 and A2 shows respectively examples of FW-FloaTEM and SW-FloaTEM data. Data in figure A1 and A2 corresponds to the resistivity model along profile BB 'in figure 7 and resistivity model along profile A- in figure 9, respectively. In each of the profile, we selected three representative decay curves (see b), c), and d) Figure A1 and A2) and corresponding data fit. The quality of data fit is represented as data residual (See Auken et. al., 2018) and its generally below 1. In SW-FloaTEM system we ignored the early time negative gates resulting due to offset geometry and very high conductivity of the saltwater.

518

519
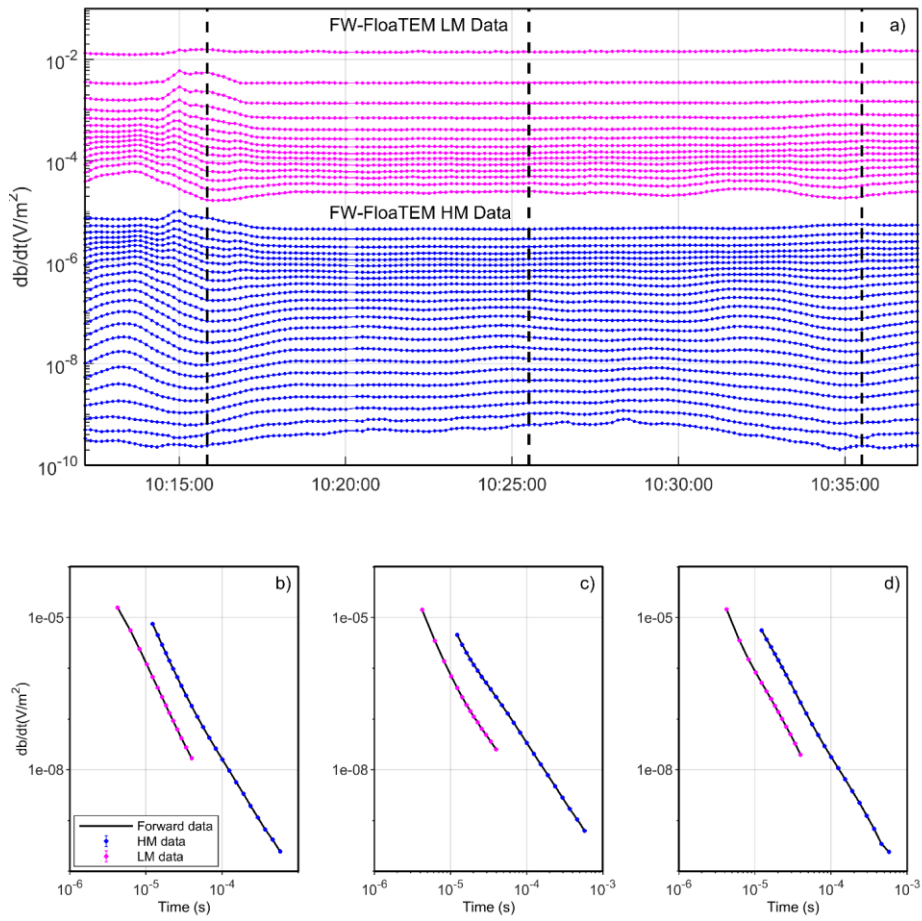
Figure A1. An example of data acquired using FW-FloaTEM system. a) shows the TEM data in profile view where each profile represents a gate; b), c) and d) are the transient decays shown respectively at three times marked as three vertical dashed lines in a).

520
521
522

523

524
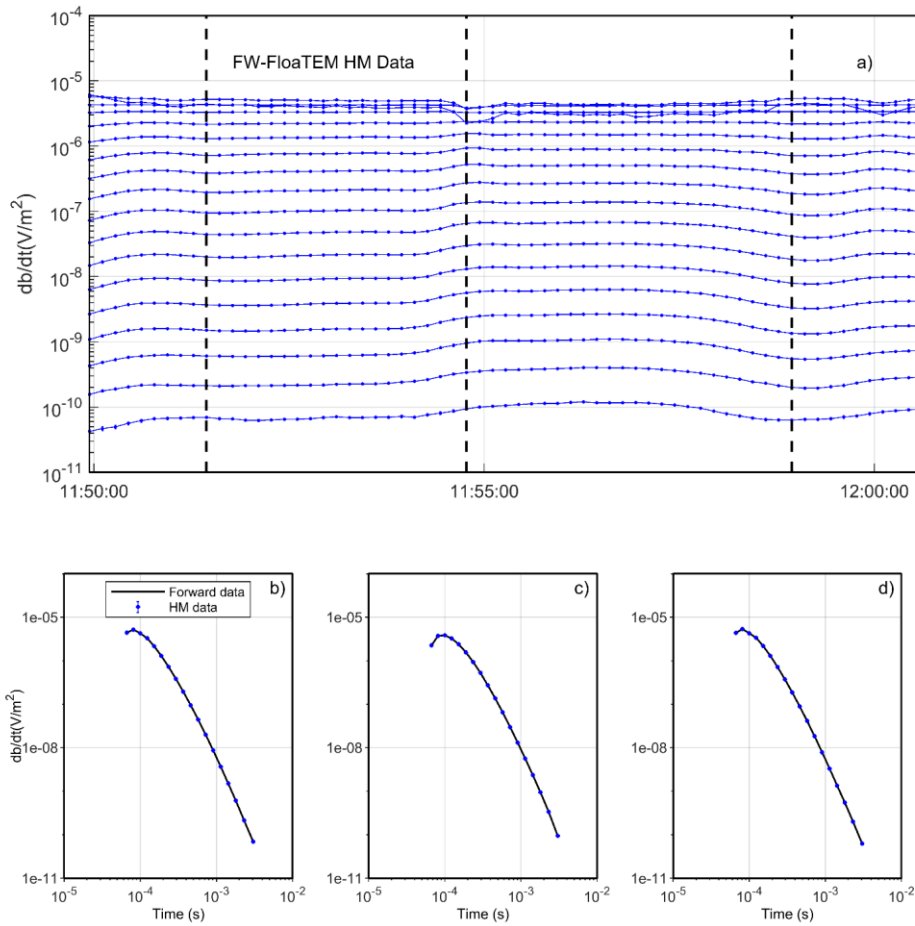
Figure A2 An example of data acquired using SW-FloaTEM system. a) shows the data in profile view where each profile represents a gate; b), c) and d) are the transient decays shown respectively at three times marked as three vertical black dashed lines in a).

528

Waveform of FW-FloaTEM and SW-FloaTEM system

In the following figures (A3-A5) we show the transmitted waveform for both LM and HM pulse used in FW-FloaTEM system and only HM waveform for SW-FloaTEM system. For each waveform we show both positive and negative pulses.
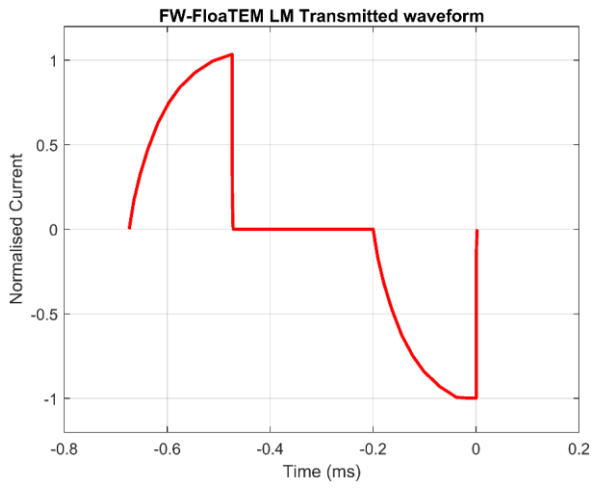
532

533   **Figure A3 LM current waveform for FW-FloaTEM system.**
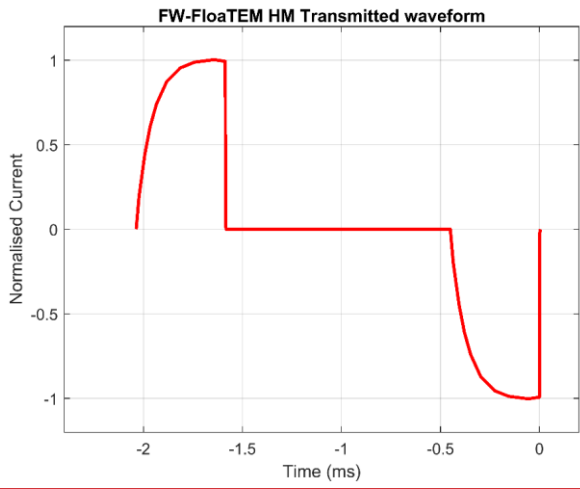
534

535   **Figure A4 HM current waveform for FW-FloaTEM system.**

536
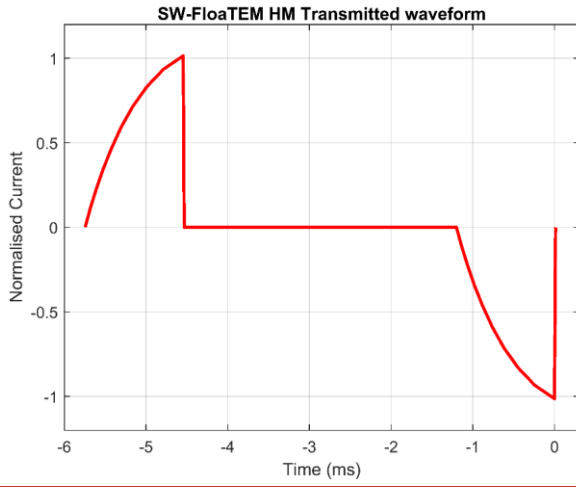
537 **Figure A5 HM current waveform for SW-FloaTEM system.**

538

539